Designing Vortex Generators for Tidal Turbine Blades

Marinos Manolesos, Nicholas Kaufmann, George Papadakis

Abstract—**Increasing tidal turbine performance through innovation is crucial if the cost of tidal energy is to become competitive compared to other sources of energy. The present investigation deals with the application of Vortex Generators (VGs) on tidal turbines in view of increasing their performance. Tidal turbine blades experience flow separation and here we examine whether passive vane VGs can be used to reduce or suppress that separated flow. VGs generate streamwise vortices that energise the boundary layer on the surface they are attached to, by bringing high momentum fluid closer to the surface. In the present investigation, a VG configuration is selected following a thorough wind tunnel campaign. It is found that sizing parameters for the tidal turbine profile are very similar to the wind turbine relevant literature. The best performing vane VG configuration had a height of 0.007c, which corresponded to half the local boundary layer height (0.5δ) for operational Reynolds numbers. A Reynolds Averaged Navier Stokes (RANS) VG modelling approach is validated against towing tank experiments and is used to simulate the flow past a tidal turbine in both model size (1:8) and full scale. The results show that VGs do suppress flow separation in both cases. However, and more importantly, it is revealed that the significance of rotational effects is such that when deciding VG placement locations, only the full-size blade should be considered. Three different VG placements are considered and the best performing one provides a power coefficient improvement of 2% is predicted at λ=3.**

Keywords — **Flow Control, Tidal Turbine, Vortex Generators.**

I. Introduction

TIDAL energy can become a valuable complementary renewable energy source, increasing the stability and reducing the total Levelized Cost of Energy[1]. However, for tidal turbines to become more attractive to investors an increase in power efficiency is required. To accelerate this process concepts developed in similar technologies, such as wind turbined, must be exploited. The more mature wind energy industry is already using Vortex Generators (VGs) either as a retrofit or in the design phase of new blades[2,3].

VGs are passive flow control devices that generate streamwise vortices that energize the boundary layer thus delaying separation[4]. They are relatively small in size (at the order of the local boundary layer height) and are attractive due to their simplicity, effectiveness and robustness.

It is currently expected that a retrofit VG installation would lead to an increase in AEP between 2% and 5% for a pitch controlled wind turbine [2,5,6]. One key point to note is the interaction between the VG induced flow and the rotational effects in the root region [7–9]. VGs are used on wind turbines too also counteract leading edge erosion effects and to suppress separation on the pressure side of blades [6,10–12], however these points are not considered here.

It was recently shown that vane VGs for tidal turbine foil profiles follow the same design rules as for wind turbine airfoils [13,14] and that VGs can be beneficial when applied on a tidal turbine blade [15,16]. For a detailed review on tidal turbine vortex generator flows, the interested reader is directed to the literature [13–16].

The present investigation aims at exploring VG placement on the blades of a three bladed tidal stream turbine and identifying the differences between model scale and full-size flows, when applied to the design of VGs. To this end, a numerical investigation was performed for a full size and a model scale blade.

The paper is organized as follows. First the numerical methodology is described followed by the description of the tidal turbine blade and the VGs considered. Then the results are given in section III and a discussion of rotational augmentation effects is given in section IV.The paper end with a discussion of the findings and concluding remarks

Dr Marinos Manolesos was a Reader in Aerospace Engineering at the School of Science and Technology at City, University of London and is now an Assistant Professor at the School of Mechanical Engineering at the National Technical University of Athens, Athens 157 80, Greece.

Dr Nicholas Kaufmann is a Tidal Turbine Engineer with Schottel Hydro GmbH, Mainzer Strasse 99, 56322 Spay/Rhin, Germany

Dr George Papadakis is an Assistant Professor at the School of Naval Architecture & Marine Engineering, National Technical University of Athens, Athens 157 80, Greece

Digital Object Identifier: https://doi.org/10.36688/ewtec-2023-343

in section V.

II. METHODOLOGY

A. Computational Fluid Dynamics Solver

The present numerical investigation utilises and in-house Reynolds Averaged Navier Stokes (RANS) solver, MaPFlow [17], developed at the National Technical University of Athens. MaPFlow is a multi-block Message Passing Interface (MPI) enabled compressible unstructured finite volume, unsteady Reynolds averaged Navier Stokes (URANS) solver. For space and time discretisation, the solver is second order accurate and can use both structured and unstructured grids. Furthermore, the discretisation technique is cell centred and for the convective fluxes, uses the Roe approximate Reimann solver for the estimation of inter cell fluxes. The solver has an in-built low Mach preconditioning to accelerate convergence in the low Mach regime, as well as an artificial compressibility (AC) option for incompressible flows. In the present study, the AC counterpart was used combined with the k-ω shear stress transport (SST) model for turbulence. Steady state simulations were performed unless otherwise stated. The specific turbulence model has been extensively used in similar flows with satisfying results [18–20].

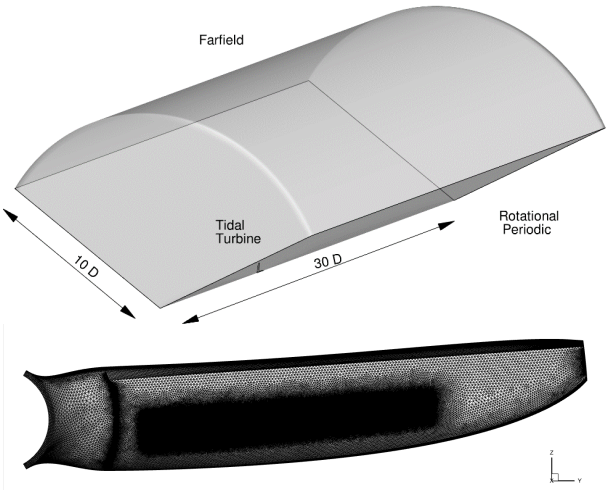

Fig. 1. (Top) The computational domain used for the CFD simulations of the tidal turbine. (b) A closer view of the tidal turbine blade surface mesh. A finer mesh is applied in the region of the Vortex Generators

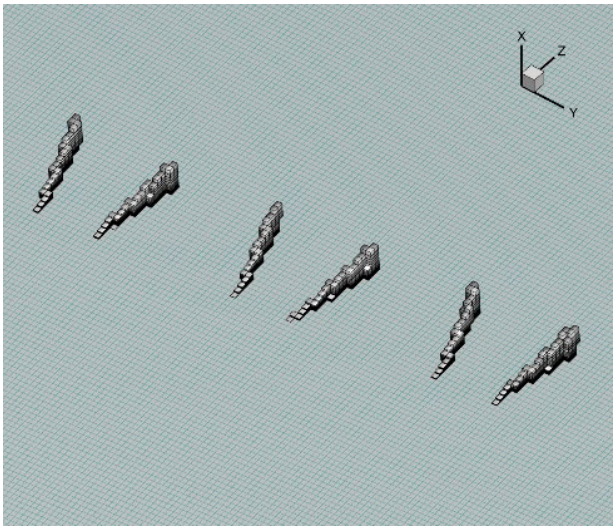

Fig. 2. Detail of the cells where the BAY model was applied.

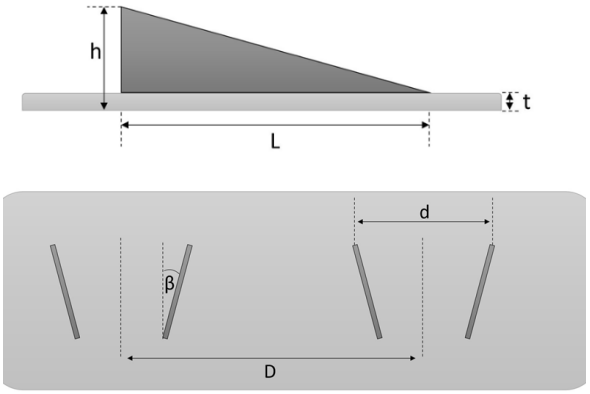

Fig. 3. Delta-shaped Vortex Generator parameters. (Top) Side view, flow coming from the right. (Bottom) Top view, flow coming from the bottom.

Regarding the tidal turbine blade simulations, the computational domain is shown in Fig. 1. The domain extends 10 rotor diameters (D) in the radial direction and 30 D in the streamwise direction. Only one blade is considered with 120^0 periodic conditions. In addition to the rotor blade, the rotor hub and a cylindrical nacelle is also modelled. The nacelle is extended up to 0.85 blade radii to ensure that any separation at the end of the nacelle will not significantly affect the flow on the blade. Further details on mesh dependence and VG modelling approach are provided in [15].

The presence of the VGs in the flow was modelled using the Bender Anderson and Yagle (BAY) model [21] in its Jirasek variation (jBAY [22]). MaPFlow and the jBAY model implementation have been thoroughly validated in [13,15,18,19,23–30]. According to the model, a source term is added to the momentum equations at the cells engulfing the VG. An example of the cells engulfing VGs on the blade is shown in Fig. 2. The force is aligning the flow to the VG direction in which case it is almost equal to zero. A detailed discussion of the model assumptions and performance is given in[26]. Approximately 15 million cells with 30 thousand cells on the blade surface were sufficient to get grid independend results regading power and torque.

B. Tidal Turbine Blade

The turbine considered is SCHOTTEL's SIT250 instream turbine in its 4m-diameter rotor version. The SIT 250 is a 85 kW horizontal axis instream turbine, designed as a

modular turbine system utilizing one drivetrain for two rotor diameters, 4 m and 6.3 m, which can be selected based upon the varying velocity frequency distributions of different deployment sites. The larger rotor diameter is suited to lower flow speed sites, whereas the smaller rotor dimeter is suited for higher resource sites. The turbine is considered both in model scale (1:8, maximum radius $R_{model} = 0.25\,m$) and full size (maximum radius $R_{FS} = 4.0\,m$) in order to analyse the scale and rotational effects on the flow over the blade and consequently on VG positioning. Results from towing tests have been used to benchmark the numerical simulations [31]. All simulations consider a $2\,m/s$ inflow velocity and a tip speed ratio range $2 < \lambda < 10$.

C. *Vortex Generators*

The vortex generator set up used in this application was developed in previous studies [13–15] and only the positioning on the blade is considered here. We considered vane type VGs and the basic sizing parameters are given in Fig. 3 and Table I.

TABLE I
VORTEX GENERATOR CONFIGURATION

VG angle, β	VG height, h/c	VG pair distance, D/h	VG distance, d/h	VG Aspect Ratio, L/h
15°	**0.7** %	7	3.5	3

III. RESULTS

A. *Model Scale Blade*

First the model scale turbine blade ($R_{model} = 0.25\,m$) is considered and the simulations are compared against experiments from the literature [31]. The agreement between measurements and simulations in terms of thrust and power coefficient is considered good, especially for $2 \leq \lambda \leq 8$, see Fig. 4.

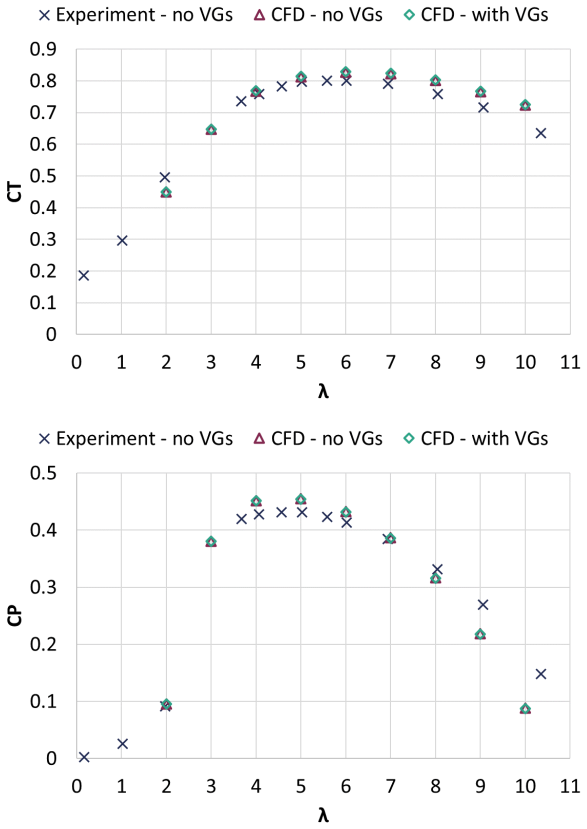

Fig. 4. Model scale blade. (Top) Thrust and (Bottom) power coefficient variation with tip speed ratio. Comparison between towing tank experiments and CFD results for an inflow velocity of $V_\infty = 2.0\,m/s$.

The surface streamlines indicate 3-dimensional separated flow in the inboard part of the blade for a tip speed ratio of $\lambda = 4$, see Fig. 5. Based on this a VG positioning is designed, as shown in the lower part of Fig. 5. The VGs are located as close to the streamwise location indicated by previous wind tunnel experiments [15] but also always upstream of the separated flow line, as indicated by the simulations shown in Fig. 5, top.

The VGs successfully limit the separated flow at this tip speed ratio. The increase in skin friction in their wake reveals they increase the velocity close to the blade surface. However, they offer timid performance improvements in terms of power increase, as shown in Fig. 4. Indeed, the pressure coefficient along the blade chord at $y = 0.31R$ barely changes by the presence of the VGs, see Fig. 6. This is due to the rotational effects present in the flow as discussed in a following section.

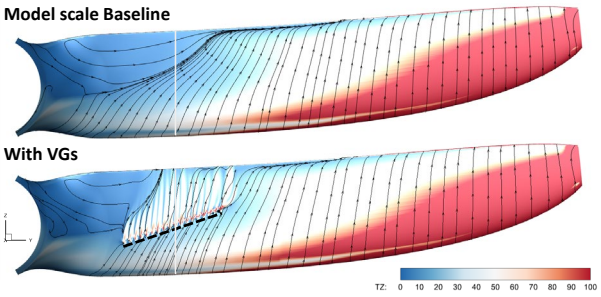

Fig. 5. Model scale blade. Chordwise skin friction (TZ) contour and skin friction lines on the blade suction side without (top) and with vortex generators (bottom) for $\lambda = 4$ and an inflow velocity of $V_\infty = 2.0\ m/s$. TZ units are N/m^2. The white vertical line and the dashed black line indicate the $y = 0.31R$ and the Vortex Generators' location, respectively. The blade rotates clockwise.

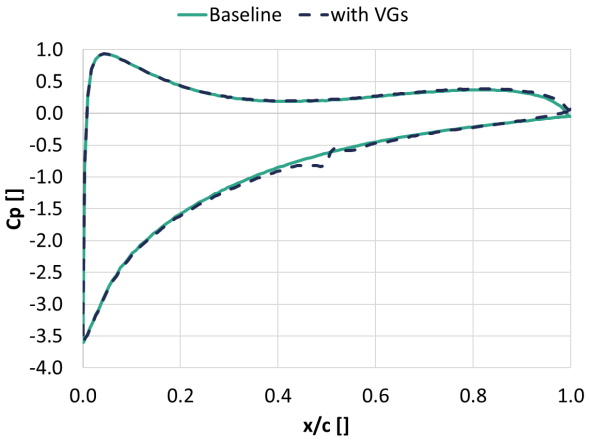

Fig. 6. Pressure coefficient distribution along the blade chord at y = 0.31R for λ = 4 and an inflow velocity of V_∞ = 2.0 m/s.

B. *Full-Size Blade*

Next the full-size blade is considered. The thrust load on the blade and the power coefficient variation with tip speed ratio is given in Fig. 7. The comparison with the model scale results reveal that the full-size blade performs significantly better at high tip speed ratios, as it operates at significantly higher Reynolds number. There is a difference at low tip speed ratio values as well, with the flow now fully attached at $\lambda = 4$ and only separating at $\lambda = 3$, see Figure 11, top.

A total of three new VG positions are considered for the full-size blade, as shown in Fig. 11 and detailed in Table II, where the basic VG parameters are given. The VG height is given with respect to the blade radius, as the chord changes along the blade radius and is not suitable as a reference quantity. In Option 1, the VGs are located on a straight line, just upstream of the separated flow, similar to the design for the model scale blade. Option 2 is as Option 1 but almost 50% higher VGs are considered. In Option 3 VGs are positioned in a 2D angled line, engulfing the separated flow region, with the height remaining as in Option 1.

TABLE II
VORTEX GENERATOR CONFIGURATION

Full-size VG option	VG height, h/R	VG pair distance, D/h	VG distance, d/h	VG Aspect Ratio, L/h
1	0.0084%	7	3.5	3
2	0.0125%	7	3.5	3
3	0.0084%	7	3.5	3

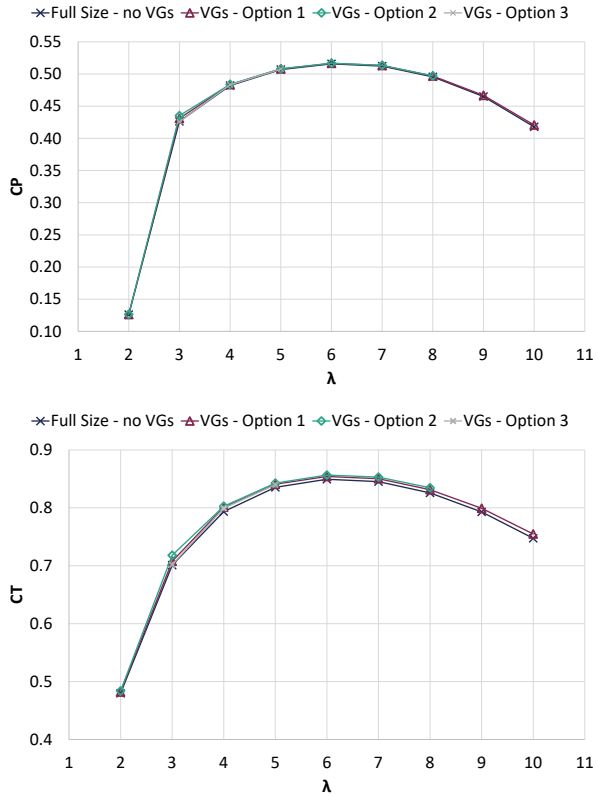

Fig. 7. Power coefficient (Top) and Thrust (Bottom) variation with tip speed ratio. Simulation results for model scale and full-size blades.

When Option 1 VGs are used, the region of separated flow is reduced in size, but not completely eliminated. Still, a power coefficient improvement of 1.05% is predicted at λ=3. This suggests that for this blade, in this case, the VG effect is not strong enough, so higher VGs (Option 2) were considered. Indeed, for Option 2, the separated flow is further reduced and the Cp gains are at the order of 2%. Option 3, where the VG lines are around the baseline separated flow region, does not provide improvements, as it appears to disturb the flow rather than aid it. Thrust increases for all VG options, across the range of tip speed ranges. Fig. 8 shows the effect of the different VG options on the turbine performance for the VG options considered here.

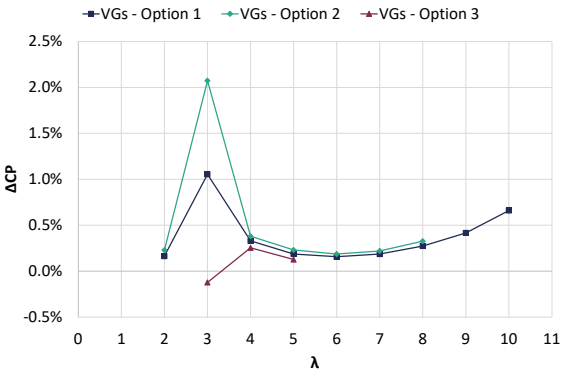

Fig. 8. Full-size blade. Change in power coefficient (C_p) due to the presence of Vortex Generators for different tip speed ratios.

IV. Rotational Augmentation

Results in the previous section highlighted how different the performance and flow over the blade differs between the full size and the scale blade. Beyond the obvious difference in Re number (O(10^5) and O(10^6) for the model scale and full-size blade, respectively), there is a significant difference in the significance of the rotational effects.

The present discussion follows the analysis presented in [8,9,32], where it has been shown that the phenomena referred to under the umbrella term 'rotational augmentation' are mainly due to the Coriolis and Centrifugal Forces acting on the flow.

The impact of rotation on the boundary layer, known as rotational augmentation, was initially explored by Himmelskamp [33]. It was observed that a propeller blade profile experienced increased lift and delayed separation compared to a non-rotating 2D airfoil. This phenomenon, referred to as the "Himmelskamp effect", was attributed to rotational forces acting on the blade's boundary layer. Fig. 9 illustrates the various mechanisms involved in this effect.

The centrifugal force, which grows stronger with increasing distance from the centre of rotation, accelerates the flow in the spanwise direction (insert frame 2 in Fig. 9) and enhances momentum within the boundary layer. As the centrifugal force intensifies towards the blade tip, more mass flow is lost from each blade section towards the tip than is received from the inner sections. This establishes a suction effect known as centrifugal pumping towards the blade tip.

Additionally, in the rotating coordinate system, the radial velocity component generates a Coriolis force that points towards the blade's trailing edge. This force reduces the extent of separated areas and energizes the chordwise boundary layer (insert frame 3 in Fig. 9), enabling it to withstand higher adverse pressure gradients [9].

To quantify this effect the Himmelskamp force, F_H, is considered, defined as the vector sum of the Coriolis and Centrifugal forces:

$$F_H = F_{Coriolis} + F_{Centrifugal} \tag{1}$$

$$F_H = -2\Omega \times V + \Omega \times (\Omega \times r) \tag{2}$$

where Ω is the angular velocity in rad/s, V is the velocity of the fluid on the rotating frame in m/s and r is the radial distance in m. It is noted that the Coriolis and Centrifugal forces have a linear and a quadratic relationship with the rotational velocity of the blade, respectively.

For the same tip speed ratio and inflow velocity ($U_\infty = 2\ m/s$), as considered here, the Centrifugal force will be greater for the model scale case by a factor equal to the inverse of the scaling factor. In the present case, the scaling factor is 1/8 so the Centrifugal force is 8 times greater in for the model blade.

The variation of the Coriolis force ratio between the model and full-size blade for λ=3 is given in Fig. 10. A single radial location is considered for clarity ($r/R = 0.31$, see also Fig. 5 and Fig. 6). As with the Centrifugal force, the Coriolis force is much larger for the model scale blade.

It is noted at this point that although the flow conditions are the same ($\lambda = 3$ and $U_\infty = 2\ m/s$) between the model scale and full-size blades, the flow is not directly comparable. In the former case the flow is partly separated while in the latter it is fully attached. In this respect, the comparison in Fig. 10 only serves as an order of magnitude reference.

V. Discussion and Conclusions

The present numerical investigation considers the flow past a tidal turbine blade in full-size and model scale (1/8) conditions. The flow differs significantly between the two cases as a result of differences in Reynolds number (one order of magnitude) and in the significance of rotational effects.

VGs were designed for both cases and were found to successfully suppress or limit separation in both cases. However, the effect in performance is very small in the model scale blade. This is because despite eliminating separation, the pressure on the blade does not change significantly when VGs are used. This is in contrast to what is expected from non-rotating airfoil flows. What happens is that in the uncontrolled case, the pressure distribution shows no plateau in the separated flow region (see Fig. 6). This is a direct outcome of the Coriolis and Centrifugal forces, which are very significant in the fast-rotating model scale blade. As such the effect of VGs is very limited.

In the full-size blade, the rotational effects are or relatively reduced importance. In this case the VGs can suppress separation and depending on the VG location can lead to a performance increase of up to 2% for $\lambda = 3$.

Regarding the VG positioning, it is found that it plays a crucial role, and a blade specific investigation should be

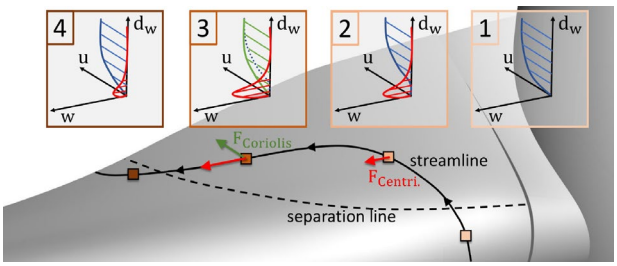

Fig. 9. Schematic description of rotational augmentation effects. The chordwise and radial boundary layer profiles are shown at different locations along a streamline: 1. Upstream of the 3D separation line; 2. Inside the 3D separated flow region where the main flow component is still in the chordwise direction, 3. Inside the 3D separated flow region where radial flow dominates; 4. Outside the 3D separated flow region, close to the trailing edge. Figure from [8].

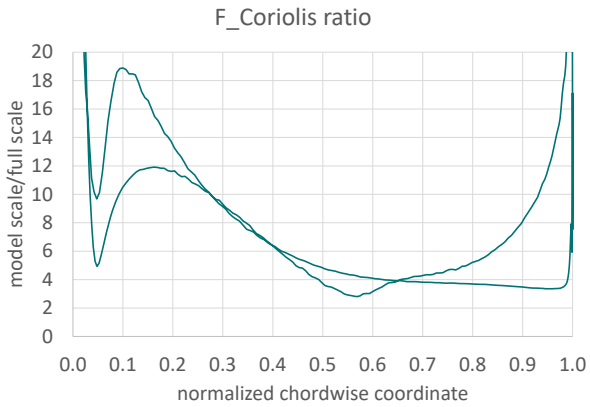

Fig. 10. Variation of the Coriolis force along the chordwise direction. The ratio $F_{model\ scale}/F_{Full-size}$ is plotted at r/R = 0.31 and for λ = 3.

followed. Utilising the fixed chordwise location and VG height suggested by 2D airfoil studies does not guarantee optimal performance.

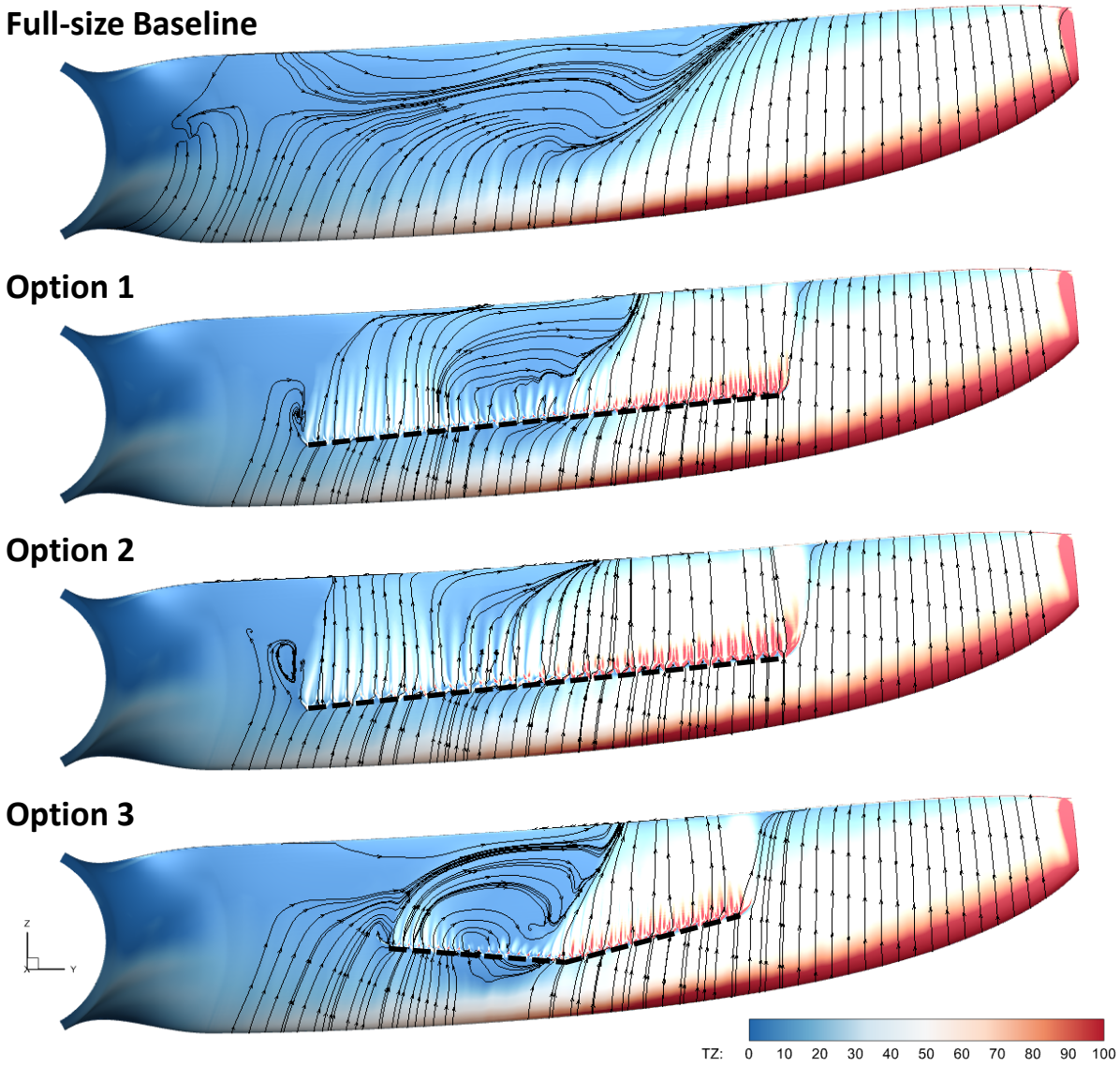

Fig. 11. Chordwise skin friction (TZ) contour and skin friction lines on the full-size blade suction side without and with vortex generators for $\lambda = 3$ and an inflow velocity of $V_\infty = 2.0\ m/s$. TZ units are N/m^2. The dashed black lines indicate the Vortex Generators' location for each of the Vortex generator Options.

REFERENCES

[1] Todeschini G, Coles D, Lewis M, Popov I, Angeloudis A, Fairley I, et al. Medium-term variability of the UK's combined tidal energy resource for a net-zero carbon grid. Energy 2022;238:121990.

[2] Hwangbo H, Ding Y, Eisele O, Weinzierl G, Lang U, Pechlivanoglou G. Quantifying the effect of vortex generator installation on wind power production: An academia-industry case study. Renew Energy 2017;113:1589–97. https://doi.org/10.1016/j.renene.2017.07.009.

[3] Soto-Valle R, Bartholomay S, Nayeri CN, Paschereit CO, Manolesos M. Airfoil Shaped Vortex Generators applied on a Research Wind Turbine. AIAA Scitech 2021 Forum, Reston, Virginia: American Institute of Aeronautics and Astronautics; 2021, p. 1413. https://doi.org/10.2514/6.2021-1413.

[4] Manolesos M, Voutsinas SG. Experimental investigation of the flow past passive vortex generators on an airfoil experiencing three-dimensional separation. J Wind Eng Ind Aerodyn 2015;142:130–48. https://doi.org/10.1016/j.jweia.2015.03.020.

[5] Troldborg N, Zahle F, Sørensen NN. Simulations of wind turbine rotor with vortex generators. J. Phys. Conf. Ser., vol. 753, IOP Publishing; 2016, p. 22057.

[6] Alber J, Manolesos M, Weinzierl G, Schönmeier A, Nayeri CN, Paschereit CO, et al. Experimental investigation of Mini-Gurney Flaps in combination with vortex generators for aerodynamic improvements of wind turbine blades. Wind Energy Sci. Conf. - EAWE, Hannover, Germany: EAWE; 2021.

[7] Zhu C, Chen J, Qiu Y, Wang T. Numerical investigation into rotational augmentation with passive vortex generators on the NREL Phase VI blade. Energy 2021;223:120089.

[8] Seel F, Lutz T, Krämer E. Numerical Study of the Unsteady Blade Root Aerodynamics of a 2MW Wind Turbine Equipped With Vortex Generators. Wind Energy Sci Discuss 2023;2023:1–28.

[9] Bangga G. Three-dimensional flow in the root region of wind turbine rotors. kassel university press GmbH; 2018.

[10] Cene A, Manolesos M, Grasso F. Aerodynamic and Aeroacoustic Measurements of the Flow Past a Very Thick Flatback Airfoil with Passive Flow Control Devices. AIAA SCITECH 2022 Forum, Reston, Virginia: American Institute of Aeronautics and Astronautics; 2022. https://doi.org/10.2514/6.2022-0279.

[11] Manolesos M, Wood B, Dinwoodie I, Celik Y, Masters I, Harrold M. Optical measurements on a 7 MW wind turbine with and without Vortex Generators. Wind Energy Sci. Conf. - EAWE, Glasgow, UK: 2023.

[12] Ravishankara AK, Bakhmet I, Özdemir H. Estimation of roughness effects on wind turbine blades with vortex generators. J. Phys. Conf. Ser., vol. 1618, IOP Publishing; 2020, p. 52031.

[13] Chng L, Alber J, Ntouras D, Papadakis G, Kaufmann N, Ouro P, et al. On the combined use of Vortex Generators and Gurney Flaps for turbine airfoils. J Phys Conf Ser 2022;2265:032040. https://doi.org/10.1088/1742-6596/2265/3/032040.

[14] Singh H, Kaufmann N, Ouro P, Papadakis G, Manolesos M. On the use of vortex generators to improve tidal turbine performance. Proc. Eur. Wave Tidal Energy Conf., EWTEC; 2021, p. 2026-1-2026–9.

[15] Manolesos M, Chng L, Kaufmann N, Ouro P, Ntouras D, Papadakis G. Using vortex generators for flow separation control on tidal turbine profiles and blades. Renew Energy 2023;205:1025–39. https://doi.org/10.1016/J.RENENE.2023.02.009.

[16] Liu Y, Zhe H, Xue Y, Tan J, Yuan P, Zhang Q. Effects of vortex generator on the hydrodynamic characteristics of hydrofoil and horizontal axis tidal turbine. Phys Fluids 2023;35.

[17] Papadakis G, Voutsinas SG. A strongly coupled Eulerian Lagrangian method verified in 2D external compressible flows. Comput Fluids 2019;195:104325. https://doi.org/10.1016/j.compfluid.2019.104325.

[18] Baldacchino D, Manolesos M, Ferreira C, González Salcedo Á, Aparicio M, Chaviaropoulos T, et al. Experimental benchmark and code validation for airfoils equipped with passive vortex generators. J Phys Conf Ser 2016;753:022002. https://doi.org/10.1088/1742-6596/753/2/022002.

[19] Manolesos M, Sørensen NN, Troldborg N, Florentie L, Papadakis G, Voutsinas S. Computing the flow past Vortex Generators: Comparison between RANS Simulations and Experiments. J Phys Conf Ser 2016;753:022014. https://doi.org/10.1088/1742-6596/753/2/022014.

[20] Baptista C, Baldacchino D, Ferreira C, van Zuijlen A, van Bussel G, Sørensen NN. Comparison of Spalart-Allmaras and k-ω SST for high-Reynolds steady airfoil simulations. 4th Symp. OpenFOAM Wind Energy, Delft, the Netherlands: 2016.

[21] Bender EE, Anderson BH, Yagle PJ. Vortex generator modeling for Navier-Stokes codes. ASME Pap FEDSM99-6919 1999.

[22] Jirasek A. Vortex-Generator Model and Its Application to Flow Control. J Aircr 2005;42:1486–91. https://doi.org/10.2514/1.12220.

[23] Diakakis K, Papadakis G, Voutsinas SG. Assessment of transition modeling for high Reynolds flows. Aerosp Sci Technol 2019;85:416–28. https://doi.org/10.1016/J.AST.2018.12.031.

[24] Prospathopoulos JM, Riziotis VA, Schwarz E, Barlas T, Aparicio-Sanchez M, Papadakis G, et al. Simulation of oscillating trailing edge flaps on wind turbine blades using ranging fidelity tools. Wind Energy 2021;24:357–78. https://doi.org/10.1002/WE.2578.

[25] Manolesos M, Papadakis G, Voutsinas SG. On the Application of the Bay Model for Vortex Generator Flows. GT2018-75217, ASME Turbo Expo, 2018. https://doi.org/10.1115/GT2018-75217.

[26] Manolesos M, Papadakis G, Voutsinas SGG. Revisiting the assumptions and implementation details of the BAY model for vortex generator flows. Renew Energy 2020;146:1249–61. https://doi.org/10.1016/j.renene.2019.07.063.

[27] Manolesos M, Papadakis G, Voutsinas SG. Assessment of the CFD capabilities to predict aerodynamic flows in presence of VG arrays. J Phys Conf Ser 2014;524:012029. https://doi.org/10.1088/1742-6596/524/1/012029.

[28] Manolesos M. Experimental and computational study of three-dimensional separation and separation control using passive vortex generators. National Technical University of Athens, 2013.

[29] Sørensen NN, Méndez B, Muñoz A, Sieros G, Jost E, Lutz T, et al. CFD code comparison for 2D airfoil flows. J. Phys. Conf. Ser., vol. 753, Institute of Physics Publishing; 2016. https://doi.org/10.1088/1742-6596/753/8/082019.

[30] Manolesos M, Papadakis G, Voutsinas SG. Experimental and computational analysis of stall cells on rectangular wings. Wind Energy 2014;17:939–55. https://doi.org/10.1002/we.1609.

[31] Kaufmann N, Carolus TH, Starzmann R. An enhanced and validated performance and cavitation prediction model for horizontal axis tidal turbines. Int J Mar Energy 2017;19:145–63. https://doi.org/10.1016/j.ijome.2017.07.003.

[32] Bangga G, Lutz T, Jost E, Krämer E. CFD studies on rotational augmentation at the inboard sections of a 10 MW wind turbine rotor. J Renew Sustain Energy 2017;9:23304.

[33] Himmelskamp H. Profile investigations on a rotating airscrew. Ministry of Aircraft Production; 1947.